JCI The Journal of Clinical Investigation

Two-photon imaging of intratumoral CD8$^+$ T cell cytotoxic activity during adoptive T cell therapy in mice

Béatrice Breart, … , Susanna Celli, Philippe Bousso

J Clin Invest. 2008;118(4):1390-1397. https://doi.org/10.1172/JCI34388.

Research Article Oncology

CTLs have the potential to attack tumors, and adoptive transfer of CTLs can lead to tumor regression in mouse models and human clinical settings. However, the dynamics of tumor cell elimination during efficient T cell therapy is unknown, and it is unclear whether CTLs act directly by destroying tumor cells or indirectly by initiating the recruitment of innate immune cells that mediate tumor damage. To address these questions, we report real-time imaging of tumor cell apoptosis in vivo using intravital 2-photon microscopy and a Förster resonance energy transfer–based (FRET-based) reporter of caspase 3 activity. In a mouse model of solid tumor, we found that tumor regression after transfer of in vitro–activated CTLs occurred primarily through the direct action of CTLs on each individual tumor cell, with a minimal bystander effect. Surprisingly, the killing of 1 target cell by an individual CTL took an extended period of time, 6 hours on average, which suggested that the slow rate of killing intrinsically limits the efficiency of antitumor T cell responses. The ability to visualize when, where, and how tumor cells are killed in vivo offers new perspectives for understanding how immune effectors survey cancer cells and how local tumor microenvironments may subvert immune responses.

Two-photon imaging of intratumoral CD8+ T cell cytotoxic activity during adoptive T cell therapy in mice

Béatrice Breart,[1,2] Fabrice Lemaître,[1,2] Susanna Celli,[1,2] and Philippe Bousso[1,2]

[1]G5 Dynamiques des Réponses Immunes, Institut Pasteur, Paris, France. [2]INSERM U668, Equipe Avenir, Paris, France.

CTLs have the potential to attack tumors, and adoptive transfer of CTLs can lead to tumor regression in mouse models and human clinical settings. However, the dynamics of tumor cell elimination during efficient T cell therapy is unknown, and it is unclear whether CTLs act directly by destroying tumor cells or indirectly by initiating the recruitment of innate immune cells that mediate tumor damage. To address these questions, we report real-time imaging of tumor cell apoptosis in vivo using intravital 2-photon microscopy and a Förster resonance energy transfer–based (FRET-based) reporter of caspase 3 activity. In a mouse model of solid tumor, we found that tumor regression after transfer of in vitro–activated CTLs occurred primarily through the direct action of CTLs on each individual tumor cell, with a minimal bystander effect. Surprisingly, the killing of 1 target cell by an individual CTL took an extended period of time, 6 hours on average, which suggested that the slow rate of killing intrinsically limits the efficiency of antitumor T cell responses. The ability to visualize when, where, and how tumor cells are killed in vivo offers new perspectives for understanding how immune effectors survey cancer cells and how local tumor microenvironments may subvert immune responses.

Introduction

Tumors rely on a wide array of mechanisms to escape destruction by infiltrating CTLs (1). Adoptive therapy relying on the transfer of a large number of activated antitumor CTLs offers a promising approach to circumvent this limitation (2) and has been shown to induce tumor regression in animal models and human clinical trials (3, 4). However, the mechanisms underlying tumor elimination after CTL transfer remain largely unknown. Studies using animal models with a deficiency in various T cell effector molecules have been instrumental in identifying the multiple roles of $CD8^+$ T cells during tumor regression. In some models, the ability of CTLs to kill (at least some) tumor or stromal cells appeared essential for tumor elimination (5–9). Other studies have noted a critical role for $CD8^+$ T cell–derived IFN-γ (10–15) and the recruitment of inflammatory cells. In addition, some CTLs act primarily by promoting the expansion of other anti-tumor T cell clones (16, 17). Finally, CTL effector functions can synergize as the production of IFN-γ increases MHC class I molecule expression on tumor cells, which thereby reduces the activation threshold required to trigger T cell cytotoxic activity (18). These studies, however, do not resolve the spatiotemporal orchestration of tumor elimination. Intravital 2-photon imaging offers the opportunity to dissect T cell behavior in lymphoid organs and was recently used to visualize intratumoral T cell motility during the course of tumor regression (19, 20). One of the critical unresolved issues is whether CTLs act primarily by killing all tumor cells or by initiating the recruitment of innate effectors that mediate tumor destruction. In addition, the rate at which tumor cells are killed by cytotoxic effectors in vivo and a possible role for this parameter in promoting tumor regression have yet to be determined. Addressing these questions has been limited in part by the technical difficulty in monitoring CTL killing activity in situ and in real time. Here, using static and intravital 2-photon imaging, we developed new approaches for assessing the cytotoxic activity of intratumoral effectors in a mouse model of solid tumor. We show that adoptive T cell therapy using in vitro primed $CD8^+$ T cells induces tumor rejection. We demonstrated that the vast majority of tumor cells are killed by CTLs, not by innate effectors, and that killing of 1 target cell occupied an individual CTL for an average of 6 hours. Interestingly, the response mounted by in vivo primed CTLs remained ineffective despite evidence of intratumoral $CD8^+$ T cell killing. Collectively, our results provide evidence that the antitumor T cell response is intrinsically limited by the extent of CTL infiltration and the slow rate of tumor cell killing by CTLs.

Results

Antigen-specific tumor regression upon adoptive transfer of in vitro primed CTLs. To visualize CTL responses against a solid tumor, we used the well-characterized EL4/EG7 subcutaneous tumor model (10, 21). C57BL/6 mice injected s.c. with EL4 tumor cells or with the OVA-expressing variant EG7 developed solid tumors that failed to be rejected in the absence of additional manipulation. Similar tumor growth patterns were observed with EL4 or EG7 tumor cells transfected with a membrane-targeted cyan fluorescent protein (mCFP) or membrane-targeted yellow fluorescent protein (mYFP), respectively. As shown in Figure 1, adoptive T cell therapy through the transfer of in vitro activated OT-I CTLs resulted in the complete regression of EG7-mYFP tumors, but had no detectable effect on the growth of EL4-mCFP tumors. Interestingly, transfer of equivalent numbers of naive OT-I T cells (even at early time points) failed to induce tumor regression with little to no tumor cell elimination being detected in tumor frozen sections (Figure 1).

Nonstandard abbreviations used: FRET, Förster resonance energy transfer; mCFP, membrane-targeted cyan fluorescent protein; mYFP, membrane-targeted yellow fluorescent protein.

Conflict of interest: The authors have declared that no conflict of interest exists.

Citation for this article: *J. Clin. Invest.* **118**:1390–1397 (2008). doi:10.1172/JCI34388.

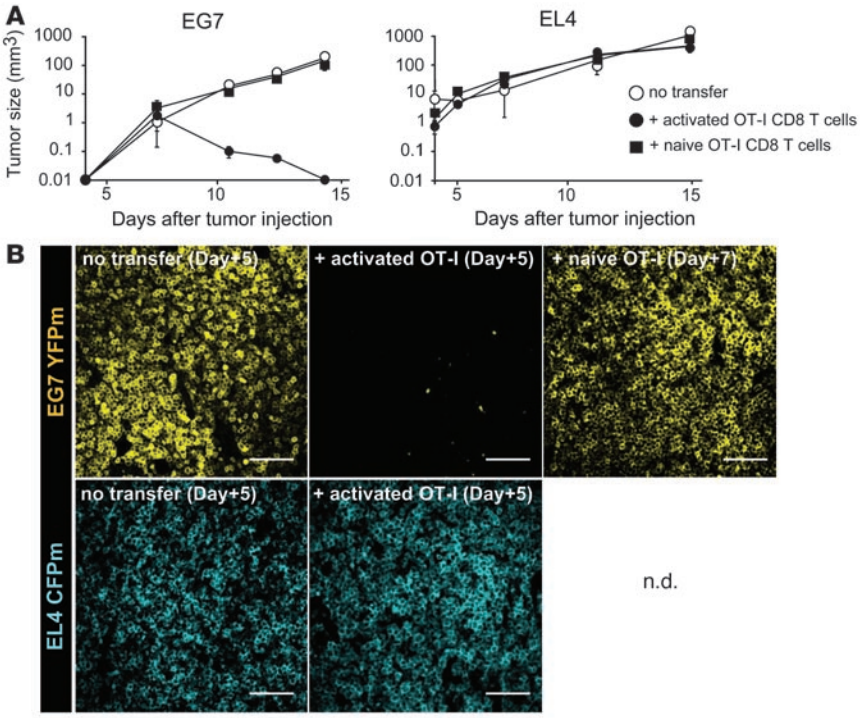

Figure 1
Antigen-specific tumor regression upon adoptive transfer of in vitro primed CTLs. C57BL/6 mice were injected s.c. with 2×10^6 EL4 tumor cells or with the OVA-expressing variant EG7 expressing mCFP or mYFP, respectively. On day 5, mice were adoptively transferred with 5×10^6 OT-I CD8$^+$ T cells that were activated in vitro for 48 hours. A second group of recipient mice were adoptively transferred with 5×10^6 naive OT-I CD8$^+$ T cells. Naive OT-I CD8$^+$ T cells were transferred on day 3 to allow additional time for in vivo activation. (**A**) Tumor growth was followed over time. In vitro, but not in vivo, primed OT-I CD8$^+$ T cells induced complete regression of EG7 tumors. (**B**) Confocal images of tumor frozen sections 5–7 days following adoptive transfer of naive or in vitro activated OT-I T cells. Most EG7-mYFP tumor cells were rapidly eliminated after transfer of activated OT-I CD8$^+$ T cells but not after transfer of naive OT-I CD8$^+$ T cells. Scale bars: 100 μm.

CTLs enhance their effector functions upon antigen recognition in the tumor environment. Nevertheless, both in vitro and in vivo primed CD8$^+$ T cells were found to infiltrate the tumor and displayed enhanced effector functions at the tumor site (Supplemental Figure 1; supplemental material available online with this article; doi:10.1172/JCI34388DS1). These hallmarks of effector activity were highly reduced or absent in OT-I T cells found in the draining lymph node or within intratumoral OT-I CTL infiltrating the non-antigen bearing EL4-mCFP tumors (Supplemental Figure 1). These results strongly suggest that transferred CTLs enhanced their effector functions at the tumor site as a result of antigen recognition. Intratumoral CTL density, however, was different. After transfer of activated OT-I T cells, the CTL density was $1.3 \pm 0.2 \times 10^4$ T cells/mm^3 on day 2 and reached $2.5 \pm 0.3 \times 10^4$ T cells/mm^3 on day 3. CTL infiltration was significantly lower and less homogenous at all time points after transfer of naive OT-I T cells, with only $0.2 \pm 0.03 \times 10^4$ OT-I T cells/mm^3 on day 7 (Figure 2, A and B).

Topography of tumor destruction upon adoptive T cell therapy. We next focused on the efficient antitumor response mounted by in vitro activated CTLs by visualizing the distribution of intratumoral OT-I CTLs during the course of tumor destruction. Two days after being transferred, CTLs accumulated in multiple discrete areas of EG7 tumors found in the vicinity of tumor microvessels (Figure 2C), their likely port of entry. On day 3, CTLs were found more evenly distributed, and most of the tumor cells had been eliminated. Tumor areas containing low numbers of CTLs usually tended to have a higher density of tumor cells (Figure 2C). On day 5, the residual mass harvested at the tumor injection site did not show any viable EG7-mYFP. These observations suggest that intratumoral CTL infiltration is initiated in multiple regions of the tumor that progressively extend and ultimately merge. Intravital 2-photon imaging performed in tumor-bearing mice 2–3 days after CTL adoptive transfer revealed that CTL located inside regions where tumor cells had been eliminated were usually motile (Supplemental Movie 1). In contrast, many CTLs were sequestered at the border of these regions, being engaged in long-lasting interactions with tumor cells (Supplemental Movie 1). Thus, intratumoral CTL dissemination occurred concomitantly with tumor cell elimination. Noteworthy, many CTLs in the vicinity of tumor cells had a high granzyme B content (Supplemental Figure 2).

The local activity of CTLs on individual tumor cells drives tumor regression. The close relationship between the topography of tumor elimination and that of CTL infiltration suggested that CTLs were playing a continuous role during tumor elimination. However, it was still unclear whether CTLs were acting by eliminating tumor cells directly or by recruiting innate effector cells that were responsible for most of the tumor destruction. To discriminate between these possibilities, we took advantage of the observation that mice injected with a mixture of EL4-mCFP and EG7-mYFP cells develop chimeric tumors (Figure 3), which are composed of small individual patches of EL4-mCFP and EG7-mYFP cells. We reasoned that if the primary effectors of tumor cell killing were the CTLs themselves, then EG7-mYFP cells should be solely targeted. In contrast, if innate effectors were largely involved in tumor destruction, both EG7-mYFP and EL4-mCFP should be destroyed. Strikingly, 3 days after injection of OT-I CTLs, virtually all EG7-mYFP patches were cleared, whereas EL4-mCFP patches appeared minimally, if at all, affected (Figure 3A). This observation was further confirmed by analyzing the tumor cell composition as a percentage (Figure 3, B and C) in absolute numbers (Supplemental Figure 3). Tumor cell mixtures containing as little as 10% EL4 tumor cells were not rejected following adoptive transfer of OT-I CTLs, which confirmed that tumor destruction proceeded with minimal nonspecific lysis. Thus, elimination of each individual tumor cell required the local action of antigen-specific CTLs, and tumor elimination occurred with little to no bystander effect.

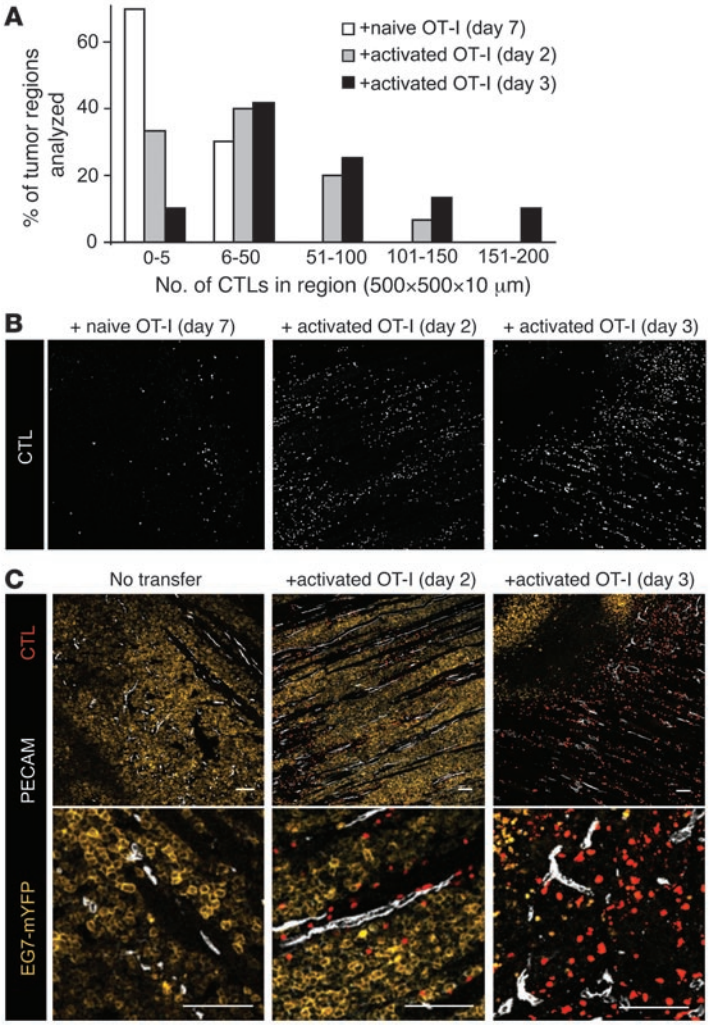

Figure 2
Visualization of intratumoral CTL dissemination during adoptive T cell therapy. (**A** and **B**) In vitro, but not in vivo, primed CTLs massively infiltrated the EG7 tumors. The distribution of intratumoral CTLs (white) was visualized and quantified on frozen sections of EG7 tumor after adoptive transfer of naive or in vitro activated OT-I CD8$^+$ T cells. (**A**) CTLs were counted in multiple individual areas of the tumor encompassing a fixed volume of 500 × 500 × 10 μm. The percentage of tumor areas containing the indicated number of CTLs is shown. The response mounted by in vivo primed OT-I CD8$^+$ T cells resulted in a lower and less homogenous CTL infiltrate than did that mounted by in vitro activated CD8$^+$ T cells at all time points analyzed. (**B**) Representative images showing CTL infiltration after transfer of naive or activated OT-I CD8$^+$ T cells. (**C**) Dissemination of in vitro primed CTLs occurred concomitantly with tumor cell elimination. Two days after adoptive transfer of in vitro activated OT-I CD8$^+$ T cells, CTLs (red) accumulated in the vicinity of tumor microvessels (white, stained for PECAM). On day 3, CTLs were more evenly distributed, and many EG7 tumor cells had been eliminated. Note that CTL-rich areas tend to have a lower density of EG7 tumor cells (yellow). Scale bars: 100 μm.

Real-time imaging of tumor cell apoptosis in vivo. To characterize the dynamics of tumor cell lysis by intratumoral CTLs, we transfected EG7 tumor cells with a fluorescent probe containing the CFP and YFP molecules linked by a peptide containing the caspase 3 cleavage motif DEVD (referred to as EG7-DEVD) (22). Apoptosis-induced caspase 3 activation resulted in substrate cleavage and subsequent Förster resonance energy transfer (FRET) disruption. As shown in Figure 4, FRET loss, which translated into a higher apoptosis index (see Methods), was readily detected in cultured EG7-DEVD tumor cells subjected to UVB irradiation or that cocultured with activated OT-I CTLs (Figure 4). Importantly, FRET loss correlated with Annexin V staining on tumor cells cocultured with OT-I CTLs (Supplemental Figure 4). No FRET changes were detected when EG7 tumor cells were transfected with a control substrate containing a noncleavable peptide DEVG (Figure 4).

Intravital 2-photon imaging of mice bearing an EG7-DEVD tumor and adoptively transferred with OT-I CTL revealed a close juxtaposition of CTLs and apoptotic tumor cells (Figure 5 and Supplemental Movie 2). As shown in Figure 5, tumor cells found in contact with CTLs were much more likely to have undergone apoptosis than were tumor cells with no CTL in their vicinity. By tracking the apoptosis index of individual tumor cells over time, we found that, of the tumor cells that remained alive during the imaging period (n = 869), only 13% were associated with CTLs (Figure 5 and Supplemental Movie 3). In contrast, 92% (n = 13) of the tumor cells that underwent apoptosis during the imaging period (as detected by FRET loss) were stably engaged by at least 1 CTL (Figure 5 and Supplemental Movie 4). This observation provides additional evidence that CD8$^+$ T cell–mediated cytotoxicity accounted for the bulk of tumor cell destruction during T cell adoptive therapy. Finally, we tracked 129 stable interactions between CTLs and live tumor cells and enumerated the number of killing events (as detected by FRET loss in individual tumor cells) as a function of the cumulated time of imaging. Using this approach, we estimated the rate of cell killing to be 1 tumor cell every 6 hours per CTL (Figure 5 and Movie 4). In summary, these results demonstrate that CTLs directly mediate tumor elimination, but require, on average, several hours to kill 1 target cell.

In vivo primed CTLs failed to control tumor growth despite displaying effective cytotoxic activity in situ. Finally, we asked whether an impaired T cell cytotoxic activity accounted for the inefficient antitumor response mounted by naive antigen-specific CD8$^+$ T cells. To this end, we visualized the response of adoptively transferred naive OT-I T cells in EG7/EL4 chimeric tumors. Although CTL infiltration was quite variable in the different regions of the

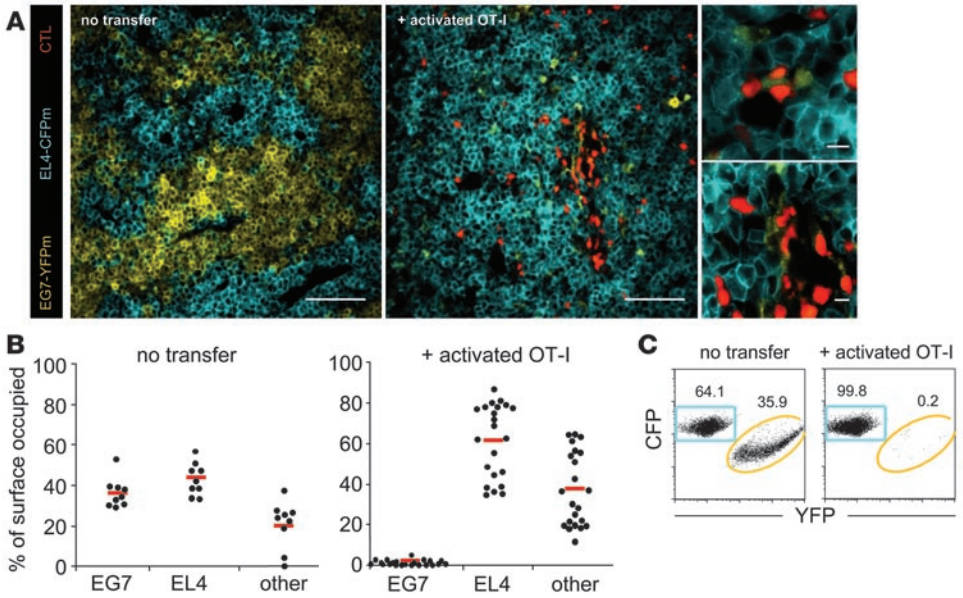

Figure 3
Direct action of CTLs on individual tumor cells drives tumor regression. Mice were injected with a mixture of EL4-mCFP and EG7-mYFP tumor cells. On day 5, some mice were adoptively transferred with 5×10^6 in vitro activated OT-I $CD8^+$ T cells. Three days after transfer, tumors were harvested, and confocal imaging was performed on frozen sections. (**A**) Mice injected with the tumor cell mixture developed chimeric tumors composed of small individual patches of EL4-mCFP and EG7-mYFP cells (left). The transfer of OT-I CTLs resulted in the clearance of EG7-mYFP patches, whereas EL4-mCFP patches appeared minimally affected (middle and right). Scale bars: 100 μm (left and middle); 10 μm (right). (**B**) The contribution of EG7-mYFP, EL4-mCFP, or other cells (i.e., nonfluorescent cells) to the overall tumor volume was determined from confocal images of frozen tumor sections. Each dot represents the value derived from an individual section. (**C**) Single-cell suspensions of tumor were analyzed by flow cytometry. The relative percentage of EG7-mYFP and EL4-mCFP cells is shown. Data are gated on tumor cells.

tumor (Figure 6A), EG7 patches were eliminated in CTL-rich areas, which was evidence that in vivo primed CTLs were not grossly impaired in their ability to kill target cells (Figure 6A, right). A similar conclusion was reached when we visualized the apoptosis of EG7-DEVD tumors induced by in vivo primed OT-I T cells, because we detected a close association between OT-I CTLs and apoptotic tumor cells (Figure 6B). Thus, the low level of $CD8^+$ T cell infiltration, rather than a defect in the cytotoxic activity, appeared to be responsible for the inefficient response mounted by in vivo primed OT-I T cells.

Discussion

Whether CTLs or other host effector cells are responsible for most of the killing during adoptive T cell therapy is controversial. Here, we used 2 novel and independent strategies to demonstrate that CTLs, but not innate effectors, were responsible for the bulk of tumor cell destruction in a model of T cell therapy (Figure 4 and Figure 6). Tumor killing occurred with minimal bystander activity (Figure 4) — a feature that may play a role in the emergence of antigen-loss variants seen after T cell therapy in some clinical trials (23). Thus, in our system, tumor regression occurred with each individual tumor cell being eliminated by CTLs. The primary role of CTLs as cytotoxic effectors does not preclude an indirect contribution of other immune cells locally. For example, evidence for intratumoral T cell–macrophage interactions have been reported (19) and could possibly enhance CTL effector functions. In addition, other cells, such as stromal cells, could be targeted as well by CTLs during this process, as reported previously (9).

In some cases, isolated CTLs were found in contact with 2 apoptotic tumor cells, which suggests that serial (24) or simultaneous (25) killing previously described in vitro may also occur in vivo. The strong enrichment for granzyme-positive CTLs at the tumor site (Figure 2 and Supplemental Figure 1) suggests that the perforin/granzyme pathway may contribute to tumor cell killing. The important role of CTL cytotoxicity revealed here by imaging approaches was surprising given that the transfer of perforin$^{-/-}$ FasL$^{-/-}$ OT-I CTLs was shown previously to efficiently induce regression of EG7 tumors (11). This observation might be explained by the redundancy of $CD8^+$ T cell cytotoxic pathways. Alternatively, a distinct mechanism for tumor regression may be involved when $CD8^+$ T cells are experimentally prevented to kill target cells. Thus, although our approach does not discriminate between the various CTL killing pathways, it provides, to our knowledge, the first direct assessment of intratumoral $CD8^+$ T cell cytotoxic activity.

Recent reports have used 2-photon microscopy to depict intratumoral T cell migration, and one study reported an example of tumor cell disintegration following interaction with a T cell. To extend these observations and characterize the dynamics of CTL killing in tumors, we combined the use of intravital 2-photon imaging and that of a fluorescent reporter of caspase 3 activity. Interestingly, we estimated the killing rate (per CTL) to be 1 tumor cell every 6 hours. Some heterogeneity in the killing ability of CTLs may exist and could not be fully appreciated here because imaging periods were limited to 1–2 hours. However, CTL-target cells almost always remained in interaction during the entire imaging

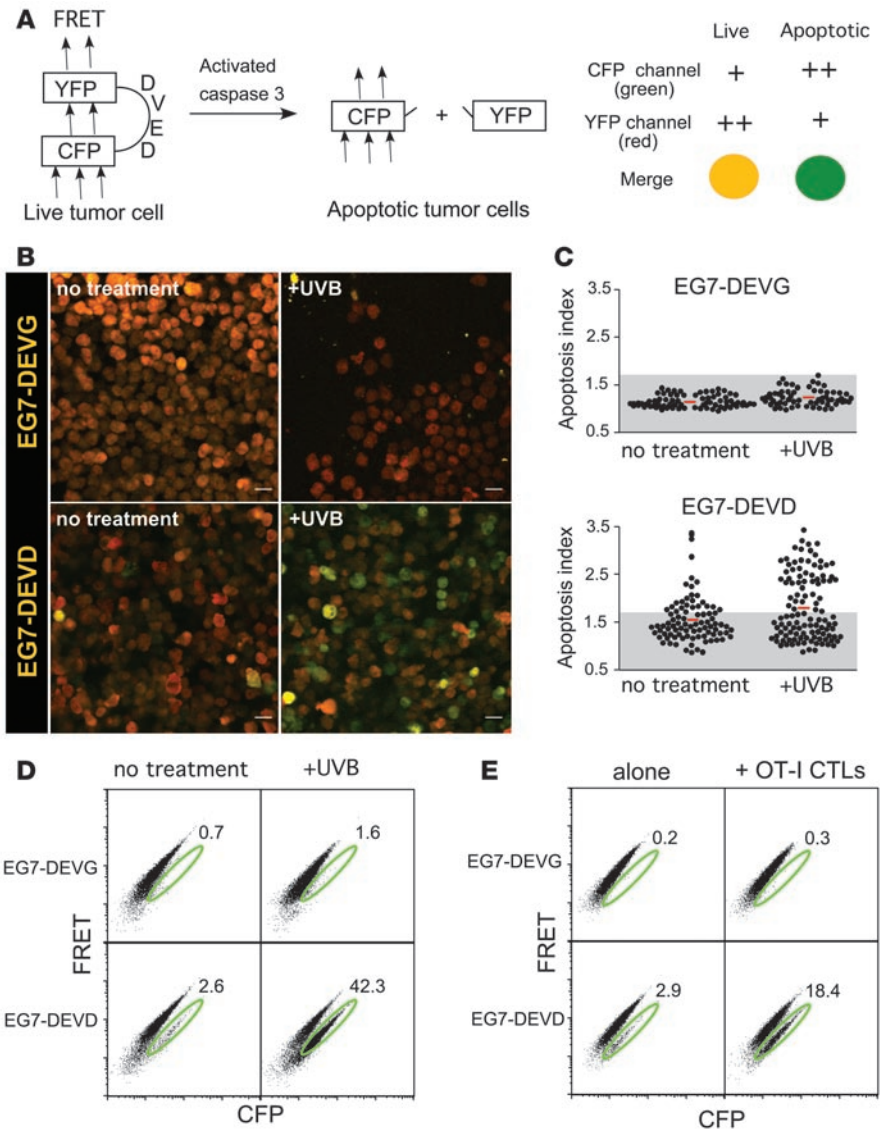

Figure 4
A fluorescent probe to track tumor cell apoptosis. (**A**) EG7 tumor cells were stably transfected with a FRET-based fluorescent probe monitoring caspase 3 activity. Briefly, CFP and YFP molecules are linked by a peptide containing the sequence DEVD, which is cleaved by activated caspase 3. EG7 cells were also transfected with a control probe (noncleavable by caspase 3) bearing a mutation in the cleavage motif (DEVG). Cleavage of the probe upon caspase 3 activation resulted in FRET disruption. Tumor cell apoptosis was monitored by 2-photon imaging by calculating the ratio of CFP to YFP emission (for the sake of clarity, this is referred to as the apoptosis index). (**B** and **C**) EG7-DEVG or EG7-DEVD tumor cells were subjected to UVB irradiation for 1 minute. Eight hours later, cells were visualized by 2-photon imaging. UVB irradiation resulted in FRET disruption in EG7-DEVD but not in control EG7-DEVG tumors cells. Scale bars: 10 μm. The apoptosis index plotted for individual tumor cells is shown. Tumor cells with a ratio greater than 1.7 were considered to be undergoing apoptosis. (**D** and **E**) Flow cytometric analysis of FRET loss in EG7-DEVD and EG7-DEVG tumor cells subjected to UVB irradiation or cocultured with activated OT-I CTLs for 5 hours. The population of EG7 tumor cells displaying FRET loss is shown in green, and the corresponding percentage is indicated.

period, confirming that during this process, CTLs are occupied for hours, not minutes. In addition, the period during which CTLs are sequestered by tumor cells often extended beyond the killing, because CTLs remained in contact with apoptotic tumor cells for up to several hours (Supplemental Movies 2 and 5).

The estimated length required for a CTL to kill a tumor cell was much longer than that described for CTLs to kill other target cells in vivo. Two-photon imaging in lymph nodes showed that CTL killing of peptide-pulsed B cells and subsequent CTL detachment from the target cell requires less than 25 minutes (26). Consistent with a rapid killing kinetic in vivo, the half-life of adoptively transferred peptide-pulsed splenocytes was found to be approximately 1 hour in lymphocytic choriomeningitis virus–immune animals (27). These differences suggest that factors such as the tumor microenvironment and/or the cell type of the target (tumor cell versus splenocytes) may influence the rate of killing. Defects in TCR proximal signaling among intratumoral $CD8^+$ T cells have been documented and could also possibly account for these differences (28). In the case of adoptive therapy with activated $CD8^+$ T cells, the relatively slow rate of killing was compensated by an elevated density of infiltrating CTLs. In other contexts, however, the kinetics of CTL-tumor cell lysis could represent a limiting factor for tumor rejection and could account for the dose- and time-dependent efficiency of adoptive T cell therapy (29, 30). This view is further supported by a pattern of response mounted by naive $CD8^+$ T cells. We found that naive antitumor $CD8^+$ T cells were primed in vivo, infiltrated the tumor, and exerted cytotoxicity in situ. Yet, they failed to eliminate the tumor, most likely because their intratumoral density was too low, which left many areas of the tumor free of CTLs. Thus, whereas tumors use many mechanisms to prevent CTL-mediated cytotoxicity, our results provide evidence that, in some cases, functional CTLs may be present at the tumor site but in insufficient numbers to induce tumor regression. The presence of a low-to-moderate number of functional CTLs could possibly contribute to a temporary state of equilibrium between the tumor and the immune response (31).

In summary, we provided direct evidence that CTLs can mediate most of the tumor cell killing during adoptive T cell therapy in situ,

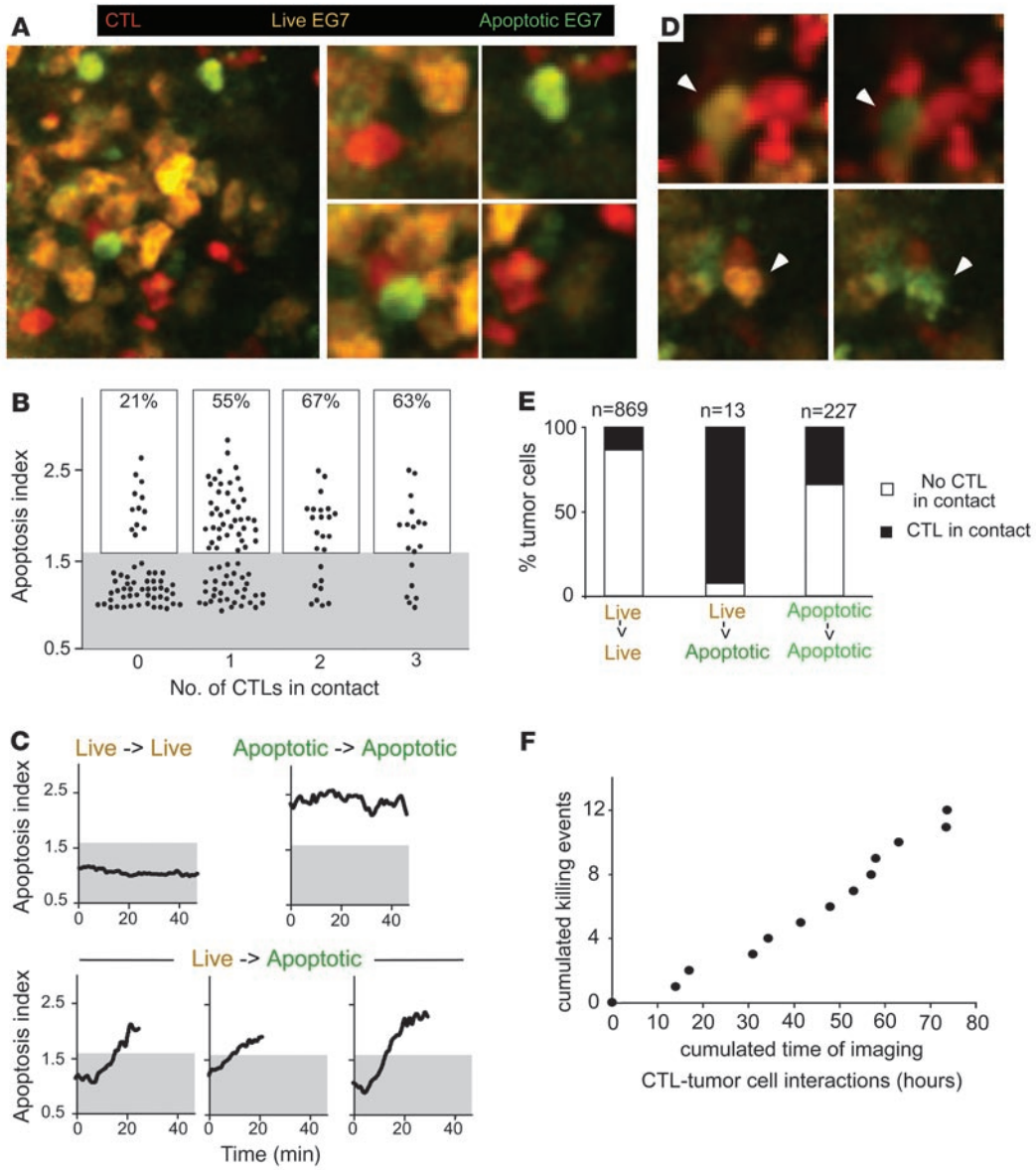

Figure 5

Dynamics of CTL-mediated tumor cell apoptosis in vivo. (**A**) Intravital 2-photon imaging of mice bearing EG7-DEVD tumors and transferred with activated GFP-expressing OT-I CTLs showed a close juxtaposition of CTLs (pseudocolored in red) and apoptotic tumor cells (green). (**B**) The apoptosis index (reflecting FRET disruption) was calculated for individual tumor cells together with the number of CTLs in contact. The percentage of tumor cells undergoing apoptosis is shown. (**C**) The apoptosis index of individual tumor cells was tracked over time. Representative tumor cells with a constant low (live→live), a high (apoptotic→apoptotic), or an increasing (live→apoptotic) apoptosis index are shown. (**D**) Examples of tumor cells undergoing apoptosis while establishing interaction with CTLs. (**E**) Tumor cells initiated apoptosis during interactions with CTLs. Individual tumor cells were divided into 3 categories on the basis of the evolution of their apoptosis index over time. The percentage of tumor cells engaged by CTLs is shown for each category. (**F**) The killing of 1 tumor cell by an individual CTL took an average of 6 hours. A total of 129 individual stable interactions between a CTL and a live tumor cell were recorded (for an average of 35 minutes each), which represented a cumulative time of imaging of 74 hours and 41 minutes. The number of killing events (as detected by FRET loss in individual tumor cells) was expressed as a function of the elapsed cumulative time of imaging. The rate of cell killing was estimated to be 1 tumor cell every 6 hours per CTL.

but at a relatively slow rate. Achieving a high and relatively uniform density of functional CTLs in the tumor could therefore be critical to counterbalance this limitation during T cell–based cancer immunotherapeutic strategies. As illustrated in the present study, real-time imaging tumor cell apoptosis in live animals should provide new opportunities for monitoring antitumor immune responses and for dissecting their modulation by the tumor microenvironment.

Methods

Mice. C57BL/6 (B6) mice were purchased from Charles River Laboratories. Transgenic mice expressing the enhanced GFP under the human ubiquitin C promoter were purchased from the Jackson Laboratory and crossed to OT-I TCR transgenic mice. Ubiquitin C–GFP × OT-I TCR transgenic mice were bred in our animal facility. All animal experiments were performed according to institutional guidelines for animal care and use.

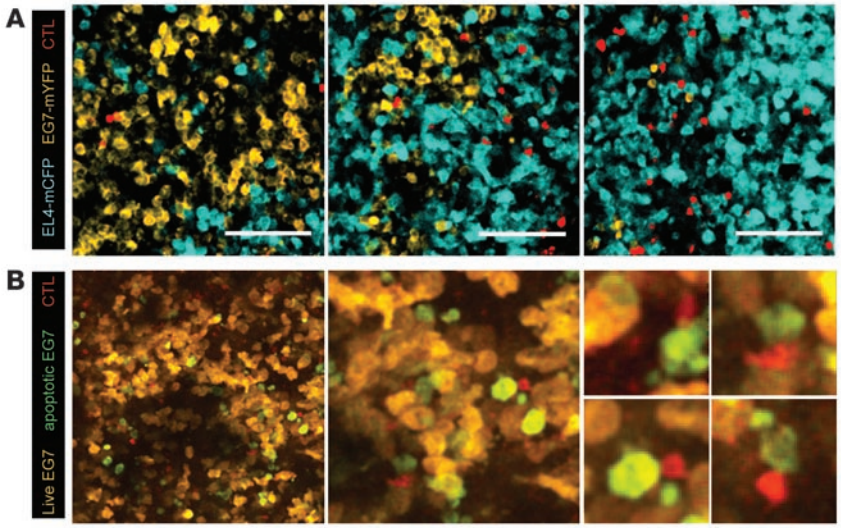

Figure 6
In vivo primed CTLs failed to control tumor growth despite exhibiting effective cytotoxic activity at the tumor site. (**A**) Naive OT-I CD8$^+$ T cells (5×10^6 cells) were adoptively transferred 3 days after the mice were injected with a mixture of EL4-mCFP and EG7-mYFP tumor cells. Representative confocal images of tumor sections indicate a distinct level of CTL infiltration. EG7 tumor cells were eliminated in the CTL-rich area, which indicated in situ cytotoxic activity (right). Little to no EG7 killing was detected in regions of the tumor with little CTL infiltration (left). Scale bars: 100 μm. (**B**) Naive OT-I CD8$^+$ T cells were adoptively transferred in mice injected with EG7-DEVD tumor cells. Representative images indicate that in vivo primed CTLs (red) were closely associated with apoptotic tumor cells (green).

Tumor cells. EL4 and EG7 tumor cell lines were purchased from the American Type Culture Collection. Constructs encoding mYFP or mCFP molecules (Clontech) or the CFP-DEVD-YFP apoptosis sensor (kindly provided by J.M Tavare, University of Bristol, Bristol, United Kingdom) were cloned in hygro pcDNA3.1 (Invitrogen). EL4 or EG7 tumor cells were transfected by electroporation, grown in complete RPMI in the presence of the appropriate selection agent, sorted using a FACS Aria (Becton Dickinson), and cloned. One clone was then selected for each transfected cell line. Tumor cells were harvested at exponential phase, and 2×10^6 tumor cells were resuspended in 50 μl of PBS and injected s.c. in the leg. Tumor volumes were recorded every 2–3 days.

T cell adoptive transfer. CD8$^+$ T cells were purified from the lymph nodes and spleens of OT-I TCR Tg or Ubiquitin C–GFP × OT-I TCR Tg mice using the depleting CD8 isolation kit (Miltenyi). For in vitro activation, OT-I T cells were stimulated using anti-CD3/anti-CD28 coated beads (Dynal) in the presence of 25 U/ml of recombinant human IL-2. Recipient mice were adoptively transferred with 5×10^6 purified naive or in vitro activated OT-I CD8$^+$ T cells.

Confocal imaging. Tumors were excised, fixed in periodate-lysine-paraformaldehyde, progressively dehydrated in sucrose gradients ranging from 10% to 30%, and then frozen in OCT compound (Tissu-Tek Sakura Finetek, Europe). Tissue sections (8-μm thick) were rehydrated and blocked with normal mouse serum and anti-CD16 mAb (eBioscience) in the presence of 1% Triton X100 (Sigma-Aldrich). Tissue sections were stained with biotin-conjugated anti-PECAM mAb (RMA) or with APC-conjugated anti-granzyme B mAb (Caltag). Sections were mounted using the Vectashield medium (Vector Laboratories) and then imaged using a confocal microscope (Zeiss). Images were processed using ImageJ software version 1.38.

Flow cytometry. Tumors and lymph nodes were digested at 37°C in RPMI 1640 containing 1 mg/ml collagenase and 0.05 mg/ml DNAse. Single-cell suspensions were subjected to intracellular staining using the Cytofix/cytoperm kit (BD Pharmingen) and either APC-conjugated anti-granzyme B mAb (Caltag) or Alexa fluor 647-conjugated anti-mouse IFN-γ mAb (clone XMG1.2; Becton Dickinson Biosciences). Cells were then analyzed with a Cyan ADP (DAKO). Data were analyzed using FlowJo software version 8.6.

Intravital 2-photon imaging of subcutaneous tumors. Mice were anesthetized and prepared for intravital imaging. Briefly, the tumor was surgically exposed and the mouse was placed on a custom-designed heated stage. To immobilize the region of interest, plaster bandages were placed on each side of the posterior leg. A coverslip was placed on top of the tumor and glued onto the plaster cast. The temperature was maintained at 37°C by a heated metal ring placed onto the coverslip and filled with water to immerge a 20X/0.95 NA dipping objective (Olympus). Two-photon imaging was performed using an upright microscope (DM 6000B) with an SP5 confocal head (Leica Microsystems). Excitation was provided by Chameleon Ultra Ti:Sapphire laser (Coherent) tuned at 880 or 940 nm. Emitted fluorescence was split using a 495-, 510-, or 560-nm dichroic mirror and passed through 465/30, 525/50, or LP560 filters (Chroma Technology) to nondescanned detectors (Leica Microsystems). Typically, 7 z-planes spaced 5 μm apart and located at least 100 μm below the tumor surface were imaged every 60 seconds. Movies were further processed using Imaris (version 5.7; Bitplane) and ImageJ software.

The apoptosis index represents the ratio of signal detected in the CFP channel to that detected in the YFP channel after normalization. In each experiment, the average value for 5 live tumor cells was used to normalize the apoptosis index to 1.

Estimation of CTL killing rate. We compiled all interactions (n = 179) between CTLs and live tumor cells observed using 2-photon imaging of mice bearing EG7-DEVD tumors and adoptively transferred with activated OT-I T cells. Overall, these individual interactions represented a cumulative time of imaging of 74 hours and 41 minutes, with an average duration of imaging of 35 minutes. A total of 12 EG7 tumor cells were seen undergoing apoptosis during the course of the imaging period (as detected by FRET disruption), which indicated that, on average, 1 tumor cell killing was detected per 6 hours of CTL-tumor cell interaction (killing rate = cumulated time of imaging/number of killing events). This calcula-

tion assumes that the kinetics of killing remain relatively constant during tumor regression.

Statistics. Data are presented as mean ± SEM. Statistical analysis was performed using the Mann-Whitney *U* test. A *P* value less than 0.01 was considered significant.

Acknowledgments

We thank J.M. Tavare for kindly providing the CFP-DEVG-YFP and CFP-DEVG-YFP constructs; M. Albert, E. Robey, and J. Di Santo for helpful comments on the manuscript; and the Plate-forme de Cytométrie and the Plate-forme d'imagerie Dynamique, Institut Pasteur. This work was supported by Institut Pasteur, INSERM, Mairie de Paris, Fondation de France, and Association pour la Recherche sur le Cancer and by a Marie Curie Excellence grant.

Received for publication November 1, 2007, and accepted in revised form January 30, 2008.

Address correspondence to: Philippe Bousso, G5 Dynamiques des Réponses Immunes, Institut Pasteur, 25 rue du Dr Roux, 75724 Paris Cedex 15, France. Phone: 33-1-45688551; Fax: 33-1-45688435; E-mail: bousso@pasteur.fr.

1. Zou, W. 2005. Immunosuppressive networks in the tumour environment and their therapeutic relevance. *Nat. Rev. Cancer.* **5**:263–274.
2. Gattinoni, L., Powell, D.J., Jr., Rosenberg, S.A., and Restifo, N.P. 2006. Adoptive immunotherapy for cancer: building on success. *Nat. Rev. Immunol.* **6**:383–393.
3. Dudley, M.E., et al. 2002. Cancer regression and autoimmunity in patients after clonal repopulation with antitumor lymphocytes. *Science.* **298**:850–854.
4. Morgan, R.A., et al. 2006. Cancer regression in patients after transfer of genetically engineered lymphocytes. *Science.* **314**:126–129.
5. Kagi, D., et al. 1994. Cytotoxicity mediated by T cells and natural killer cells is greatly impaired in perforin-deficient mice. *Nature.* **369**:31–37.
6. Smyth, M.J., Kershaw, M.H., Darcy, P.K., and Trapani, J.A. 1998. Adoptive transfer: the role of perforin in mouse cytotoxic T lymphocyte rejection of human tumor xenografts in vivo. *Xenotransplantation.* **5**:146–153.
7. Caldwell, S.A., Ryan, M.H., McDuffie, E., and Abrams, S.I. 2003. The Fas/Fas ligand pathway is important for optimal tumor regression in a mouse model of CTL adoptive immunotherapy of experimental CMS4 lung metastases. *J. Immunol.* **171**:2402–2412.
8. Peng, L., et al. 2000. T cell-mediated tumor rejection displays diverse dependence upon perforin and IFN-gamma mechanisms that cannot be predicted from in vitro T cell characteristics. *J. Immunol.* **165**:7116–7124.
9. Spiotto, M.T., Rowley, D.A., and Schreiber, H. 2004. Bystander elimination of antigen loss variants in established tumors. *Nat. Med.* **10**:294–298.
10. Helmich, B.K., and Dutton, R.W. 2001. The role of adoptively transferred CD8 T cells and host cells in the control of the growth of the EG7 thymoma: factors that determine the relative effectiveness and homing properties of Tc1 and Tc2 effectors. *J. Immunol.* **166**:6500–6508.
11. Hollenbaugh, J.A., Reome, J., Dobrzanski, M., and Dutton, R.W. 2004. The rate of the CD8-dependent initial reduction in tumor volume is not limited by contact-dependent perforin, Fas ligand, or TNF-mediated cytolysis. *J. Immunol.* **173**:1738–1743.
12. Blohm, U., Potthoff, D., van der Kogel, A.J., and Pircher, H. 2006. Solid tumors "melt" from the inside after successful CD8 T cell attack. *Eur J. Immunol.* **36**:468–477.
13. Nagoshi, M., Sadanaga, N., Joo, H.G., Goedegebuure, P.S., and Eberlein, T.J. 1999. Tumor-specific cytokine release by donor T cells induces an effective host anti-tumor response through recruitment of host naive antigen presenting cells. *Int. J. Cancer.* **80**:308–314.
14. Barth, R.J., Jr., Mule, J.J., Spiess, P.J., and Rosenberg, S.A. 1991. Interferon gamma and tumor necrosis factor have a role in tumor regressions mediated by murine CD8+ tumor-infiltrating lymphocytes. *J. Exp. Med.* **173**:647–658.
15. Schuler, T., and Blankenstein, T. 2003. Cutting edge: CD8+ effector T cells reject tumors by direct antigen recognition but indirect action on host cells. *J. Immunol.* **170**:4427–4431.
16. Nagoshi, M., et al. 1998. Successful adoptive cellular immunotherapy is dependent on induction of a host immune response triggered by cytokine (IFN-gamma and granulocyte/macrophage colony-stimulating factor) producing donor tumor-infiltrating lymphocytes. *J. Immunol.* **160**:334–344.
17. Lurquin, C., et al. 2005. Contrasting frequencies of antitumor and anti-vaccine T cells in metastases of a melanoma patient vaccinated with a MAGE tumor antigen. *J. Exp. Med.* **201**:249–257.
18. Meunier, M.C., et al. 2005. T cells targeted against a single minor histocompatibility antigen can cure solid tumors. *Nat. Med.* **11**:1222–1229.
19. Mrass, P., et al. 2006. Random migration precedes stable target cell interactions of tumor-infiltrating T cells. *J. Exp. Med.* **203**:2749–2761.
20. Boissonnas, A., Fetler, L., Zeelenberg, I.S., Hugues, S., and Amigorena, S. 2007. In vivo imaging of cytotoxic T cell infiltration and elimination of a solid tumor. *J. Exp. Med.* **204**:345–356.
21. Moore, M.W., Carbone, F.R., and Bevan, M.J. 1988. Introduction of soluble protein into the class I pathway of antigen processing and presentation. *Cell.* **54**:777–785.
22. Tyas, L., Brophy, V.A., Pope, A., Rivett, A.J., and Tavare, J.M. 2000. Rapid caspase-3 activation during apoptosis revealed using fluorescence-resonance energy transfer. *EMBO Rep.* **1**:266–270.
23. Yee, C., et al. 2002. Adoptive T cell therapy using antigen-specific CD8+ T cell clones for the treatment of patients with metastatic melanoma: in vivo persistence, migration, and antitumor effect of transferred T cells. *Proc. Natl. Acad. Sci. U. S. A.* **99**:16168–16173.
24. Poenie, M., Tsien, R.Y., and Schmitt-Verhulst, A.M. 1987. Sequential activation and lethal hit measured by [Ca2+]i in individual cytolytic T cells and targets. *EMBO J.* **6**:2223–2232.
25. Wiedemann, A., Depoil, D., Faroudi, M., and Valitutti, S. 2006. Cytotoxic T lymphocytes kill multiple targets simultaneously via spatiotemporal uncoupling of lytic and stimulatory synapses. *Proc. Natl. Acad. Sci. U. S. A.* **103**:10985–10990.
26. Mempel, T.R., et al. 2006. Regulatory T cells reversibly suppress cytotoxic T cell function independent of effector differentiation. *Immunity.* **25**:129–141.
27. Barchet, W., et al. 2000. Direct quantitation of rapid elimination of viral antigen-positive lymphocytes by antiviral CD8(+) T cells in vivo. *Eur. J. Immunol.* **30**:1356–1363.
28. Koneru, M., Schaer, D., Monu, N., Ayala, A., and Frey, A.B. 2005. Defective proximal TCR signaling inhibits CD8+ tumor-infiltrating lymphocyte lytic function. *J. Immunol.* **174**:1830–1840.
29. Hanson, H.L., et al. 2000. Eradication of established tumors by CD8+ T cell adoptive immunotherapy. *Immunity.* **13**:265–276.
30. Cordaro, T.A., et al. 2000. Tumor size at the time of adoptive transfer determines whether tumor rejection occurs. *Eur. J. Immunol.* **30**:1297–1307.
31. Dunn, G.P., Old, L.J., and Schreiber, R.D. 2004. The three Es of cancer immunoediting. *Annu. Rev. Immunol.* **22**:329–360.